The Modular Current-Fed High-Frequency Isolated Matrix Converters for Wind Energy Conversion

Yang Xu, *Student Member, IEEE*, Zheng Wang, *Senior Member, IEEE*, Pengcheng Liu, *Student Member, IEEE*, Qiang Wei, Fujin Deng, *Senior Member, IEEE*, and Zhixiang Zou, *Senior Member, IEEE*

***Abstract*—In this article, a modular current-fed high-frequency transformer isolated matrix converters (CF-HFT-MC) based wind energy conversion system (WECS) is proposed. The CF-HFT-MC module utilizes the high-frequency transformer instead of the line-frequency input transformer, and eliminates the bulky and vulnerable electrolytic capacitors in the WECS. Therefore, the power density, reliability and efficiency of WECS can be increased. Moreover, single-stage power conversion and soft-switching can be achieved in the CF-HFT-MC modules, which can reduce the losses of the system. With the function of electric isolation, the wind turbines can be connected in series through the proposed CF-HFT-MC modules. Thus, the total dc output voltage is increased, which enables the offshore wind farm to be integrated to the current-source-converters based HVdc transmission directly. The modulation, control scheme and power sharing method are analyzed and designed for the proposed CF-HFT-MC based WECS in this article. Both the simulations and the experiments are given to verify the effectiveness of the proposed system.**

***Index Terms*—Current source converter, high-frequency-transformer, matrix converter, modular converter, wind energy conversion system.**

I. Introduction

THE WIND energy has been one of the most important renewable energy sources for saving use of fossil energy and reducing the carbon emission [1]. The wind energy conversion systems (WECS) can be classified into two categories: the onshore WECS and the offshore WECS. Compared with the onshore WECS, the offshore WECS has the advantages including the abundant wind resources, the higher and steadier wind speed, and little impact on the environment [2]. The offshore wind farms could be connected to the main grid through either high-voltage alternating current (HVac) transmission system or high-voltage direct current (HVdc) transmission system [3]. The HVac transmission system has a simple structure and control algorithm. But it uses the ac cables as the transmission line, which has larger capacitance to ground compared with overhead ac lines. The existence of capacitive current limit the transfer capability and causes high conduction losses. Therefore, the HVac system is usually used in wind farms whose offshore distance is less than 50 km [4]. Compared with the HVac transmission, the HVdc transmission system has lower grounding current through the cable, which allows the transmission distance longer than 50 km for the offshore wind.

According to the connection method of the wind turbines, the off-shore HVdc systems can be further divided into two groups: The first group is the parallel-connected configuration of wind turbines, it has been already commercialized in the market [5]. The output voltages of multiple wind turbines are stepped up by low-frequency step-up transformers in wind farms. Thus, the power of wind turbines is collected in parallel with the medium-voltage ac bus, and then transmitted to the HVdc system by another step-up transformer and a rectifier. However, multiple stages of power conversion will reduce the efficiency and reliability of the WECS. Moreover, the low-frequency step-up transformer will increase the weights and footprints of WECS, which are of great importance for offshore infrastructures. The second group is to utilize the series-connected power converters for reaching the HVdc voltage level directly by using the cascaded configuration [6]. Consequently, the offshore substations can be eliminated, and the efficiency, power density, and cost will be improved.

Currently, the voltage-source converters (VSCs) have dominated the market of offshore WECS applications. Both two-level VSCs and multilevel VSCs have been widely studied for the HVdc-WECS [7]–[9]. The large capacitors are usually required in the dc link of both the two-level and the multilevel VSCs to stabilize the dc-link voltages. The dc-link capacitors used are heavy and bulky, which will reduce the power density of the converter. Moreover, the electrolytic dc-link capacitors suffer from the high failure rate [10]. The temperature limitation of electrolytic capacitors challenges the thermal design of the WECS.

On the other hand, the current-source converters (CSCs) replace the capacitors with chokes in dc link, and therefore, offer a higher reliability and a higher operation temperature limitation

Manuscript received June 8, 2021; revised September 14, 2021; accepted October 22, 2021. Date of publication October 27, 2021; date of current version December 31, 2021. This work was supported in part by the Shenzhen Science and Technology Innovation Committee under Grant JCYJ20180306174439784 and in part by the Postgraduate Research and Practice Innovation Program of Jiangsu Province under Grant KYCX21_0098. Recommended for publication by Associate Editor B. Singh. *(Corresponding author: Zheng Wang.)*

Yang Xu, Pengcheng Liu, Fujin Deng, and Zhixiang Zou are with the School of Electrical Engineering, Southeast University, Nanjing 210096, China (e-mail: 230208298@seu.edu.cn; 230189237@seu.edu.cn; fdeng@seu.edu.cn; zzou@ieee.org).

Zheng Wang is with the School of Electrical Engineering, Southeast University, Nanjing 210096, China also with the Shenzhen Research Institute, Southeast University, Shenzhen 211189, China (e-mail: zwang@eee.hku.hk).

Qiang Wei is with the Department of Electrical Engineering, Lakehead University, Thunder Bay, ON P7B 5E1, Canada (e-mail: qwei@lakeheadu.ca).

Color versions of one or more figures in this article are available at https://doi.org/10.1109/TPEL.2021.3123204.

Digital Object Identifier 10.1109/TPEL.2021.3123204

[11], [12]. Different from VSCs, the power switches of CSCs require the reversely voltage-blocking ability. The symmetric gate-commutated thyristor devices have been utilized in high-power CSC based electrical machine systems with low switching frequencies [13]. Recently, the studies have been extended to the CSCs based electrical machine systems with high-frequency devices such as IGBTs and wide-bandgap (WBG) MOSFETs, where the diodes are required to be connected to the switches in series to offer the reversely voltage-blocking ability [14], [15]. The monolithic WBG devices based bidirectional power switches have also been applied in the current-source inverter based motor drive systems to reduce the conduction losses [16], [17].

The CSCs-based configurations include the line-commutated converter (LCC) and pulse-width-modulation (PWM) CSC. The LCC based HVdc system has advantages including the large transmission capacity, low system conversion loss, and high reliability, which has been put in service on land for more than five decades [18]. However, the LCC based HVdc requires large passive filters to mitigate the lower order harmonics, which will increase the footprints and weights of the power conversion system. Additionally, the dynamic response is slow and the control of active and reactive powers is coupling. The ac voltage source is also required to help commutation of thyristors used in the system. Therefore, the LCC based HVdc is less attractive in the offshore wind farms.

The PWM CSC is considered as a promising solution for offshore wind systems with the friendly grid waveforms, controllable power factor, and high reliability [2]. A back-to-back CSC is used to convert the power to the grid from a single wind turbine, and the energy storage is added to smooth the fluctuating wind power [19]. In [20], the control strategy is developed for fast dynamic response and minimum dc-link current for the CSC based WECS. In [21], the cascaded PWM CSCs are proposed for both generator and grid side of WECS, so that dc voltages are increased and the HVdc transmission is implemented. A parallel configuration PWM CSC based HVdc system is further proposed in [22] to reduce the conduction losses and improve the flexibility of the system. However, the low-frequency transformers are required to solve the issue of insulation for the wind turbines with cascaded CSCs. Compared with the low-frequency transformer, the medium-frequency transformers or high-frequency transformers are with advantages of smaller, controllable, and flexible [23]. The medium-frequency transformer based cascaded wind turbines have been proposed for offshore wind applications with CSCs [24], [25]. Thus, the bulky size of low-frequency transformer can be saved, while the cascaded WECS can be achieved for HVdc transmission. However, the uncontrolled rectifier bridge is used to convert the ac output voltage of wind turbine to dc voltage, and the dc capacitors are required for decoupling and stabilizing the dc-link voltage. Therefore, the lifetime and reliability of the converter will be reduced.

The matrix converter (MC) is a unique power converter, which can convert the input ac voltage to the output ac voltage directly without intermediate dc link. The absence of electrolytic capacitors can further improve the reliability and prolong the service time of the system. With the development of high-frequency switching devices and magnetic components, the high-frequency-transformer isolated matrix converter has been studied in the grid-tied converter [26], energy storage [27], and wireless power transfer [28], where the H-bridge is used to connect the high-frequency link and the dc source or load. To further improve the reliability, both unidirectional and bidirectional current-fed high-frequency-transformer isolated matrix converter (CF-HFT-MC) systems have been proposed [26], [29]. The soft-switching can be realized for switches in direct matrix converter (DMC), and the power density and efficiency are higher compared with the DAB-based two stage system. In [30], the CF-HFT-MC has been proposed for wind turbine applications. However, the previous study of CF-HFT-MC system has been limited to a single module. Due to the requirements of large capacity and high voltage for offshore wind farms, the modular CF-HFT-MC based WECS and HVdc transmission system is to be explored.

For WECS, the electric power is usually generated from the wind. Therefore, the unidirectional power flow is enough except for some special functions. In fact, the bidirectional power control capability of a single CF-HFT-MC module has been studied and verified in [26]. By replacing the diode bridge rectifier with full bridge converter, the bidirectional power flow capability can be achieved in the proposed configuration. The purpose of this article is to study the modular IPOS configuration with current-fed isolated matrix converter. Therefore, the diode bridge rectifier is employed for the sake of brevity. Compared with the conventional VSC based two-stage conversion system, the matrix converter has the following merits: The first one is the elimination of dc-link capacitor, which can increase the reliability and power density. According to [31], the fault in dc-link capacitor occupies 40% of the total failures in the power converter of WECS. Furthermore, the three-phase sinusoidal voltage can be produced on the terminal of the generator. In the VSC based drive system, the PWM voltage is applied on the generator windings. The high du/dt of the voltage leads to serious problems including winding insulation and bearing failures [32]. When the power converter is put on the base of WECS, the du/dt issue becomes more challenging with long-cable connection. Besides, it has been disclosed that the system efficiency could be improved with the single-stage power conversion though more power devices are used in the matrix converter [30]. The stiffness provided by energy storage element is crucial in a WECS where the nature of wind is uncertain. Although the dc-link capacitor is eliminated in the matrix on the generator side, the dc choke still exists on the output dc side. The dc choke can help smooth the power fluctuation of the wind, which is actually similar with the current-source-converter based WECS. Compared with the electrolytic capacitors, the dc choke provides the higher reliability.

As the power rating of the generator increases, the power devices have to stand higher current or voltage stresses. Meanwhile, it is difficult for the design and construction of HFT considering the large power capacity and high insulation level. Consequently, the connection of power converters in parallel or series is a possible solution to distribute the large power from

the generator. In this article, the modular design is introduced with input-parallel output-series (IPOS) configuration for HVdc system. The system complexity could be reduced with the modular design. Furthermore, the IPOS configuration increases the total dc-link voltage of the CF-HFT-MC modules and helps eliminate the offshore high-voltage dc–dc converter [33]. Hence, the proposed modular design and IPOS configuration could help reduce the system complexity although the device count of WECS is increased for high power ratings. In addition, the high-frequency transformer is used to provide electric isolation and voltage matching between the ac side and the dc side.

The line-frequency transformer in the conventional WECS mainly provides the function of galvanic isolation and voltage scaling which offers low conduction losses. In previous pieces of literature, it has been disclosed that the power loss is a common issue faced by the HFT based high-power converters such as the solid-state transformer [34]. Nevertheless, with the development of advanced nanocrystalline materials for HFT and WBG devices for the power converters, the overall efficiency of the HFT based power conversion system has been increased greatly. Furthermore, the single-stage power conversion of DMC could potentially reduce the losses compared with traditional DAB based two-stage converters [30]. Third, the IPOS configuration can eliminate the use of the offshore substation dc–dc converters in the dc collecting grid [33]. Therefore, the losses in the offshore substation dc–dc converters can be reduced.

Compared with the conventional VSC based HVdc system [33], there are three attracting features of the proposed configuration when considering the reliability and the service life. The first is that the dc-link capacitor is eliminated in the proposed system, which dominates the life cycle of the power converters in WECS [35]. The aluminum electrolytic capacitor is commonly used in the dc-link for lower cost and higher power density. But it is vulnerable and sensitive to critical stressors, including temperature, vibration, and humidity. Instead of electrolytic capacitor, the inductor is used in the dc-link for the proposed configuration, which is resistant to the thermal shock and has a higher reliability. The second feature is the three-phase sinusoidal voltages on the terminal of the generator. In the VSC based drive system, the PWM voltage waveforms on the generator windings bring in serious problems including winding insulation and bearing failures [32]. This issue becomes more challenging when the power converter is put on the base of wind turbine and the long cable is used for connection. Last but not the least, the modular design in the proposed WECS can also enhance the system reliability. When the fault occurs in the DMC, the faulty module will be isolated from the system. The left healthy modules can still carry the power from the generator.

Compared with the existing WECS, the contributions and differences of the proposed modular CF-HFT-MC based WECS can be summarized as: First, the use of electrolytic capacitors is avoided completely in the CF-HFT-MC modules, and the reliability and service life of the converter can be improved. Second, the single-stage conversion and soft-switching are achieved for the CF-HFT-MC, which can help increase the efficiency of the system. Third, the dedicated modulation strategy and control scheme have been proposed for the CF-HFT-MC based WECS

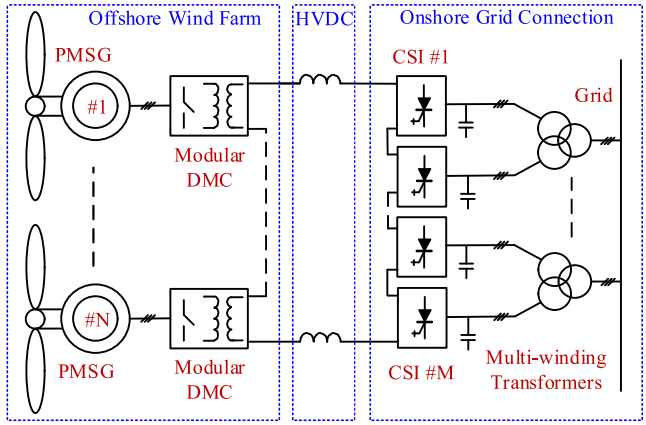

Fig. 1. Overall structure of the cascaded HVdc system.

system, where the IPOS connection is employed to integrate the low-voltage wind turbines into the HVdc transmission system. Not only the safe commutation is provided for the CF-HFT-MC, but also even power distribution and balanced output voltage are achieved for multiple power modules.

The rest of this article is organized as follows. The configuration of the proposed CF-HFT-MC based WECS is described in Section II. In Section III, the operation principles of the CF-HFT-MC system, including the modulation scheme, the commutation and the duty loss compensation, are analyzed in detail. Then, the control schemes of both the generator-side converter and the grid-side converter, in particular for the power sharing and voltage balance control of CF-HFT-MC modules, are presented in Section IV. In Section V, both the simulations and the experiments on a laboratory prototype are given to verify the effectiveness of the proposed system. Finally, Section VI concludes this article.

II. Configuration of the Proposed WECS

Fig. 1 shows the overall structure of modular DMC-based offshore WECS and HVdc transmission system. The proposed WECS in the offshore wind farm is connected in cascade to construct the high-voltage dc output terminal. The medium-voltage current-source inverters (CSIs) are also connected in cascade and transfer the power to the grid through multi-winding transformers in the onshore station. Through the high-power dc choke and transmission lines, the converters in the offshore wind farm and the onshore transformer station are connected. As shown in Fig. 2, only one WECS fed by the proposed modular high-frequency isolated DMC is studied in this article for simplicity. The inputs of modular DMCs are connected in parallel on the generator side to satisfy the operation requirements of large-capacity wind turbines under limited voltages. On the other hand, the dc outputs are connected in cascade to increase the dc output voltage for HVdc transmission. The working principle and control scheme for one wind turbine could be extended to multiple wind turbines in Fig. 1.

Fig. 3 shows the detailed schematic of one current-fed high-frequency isolated DMC module, which consists of three main

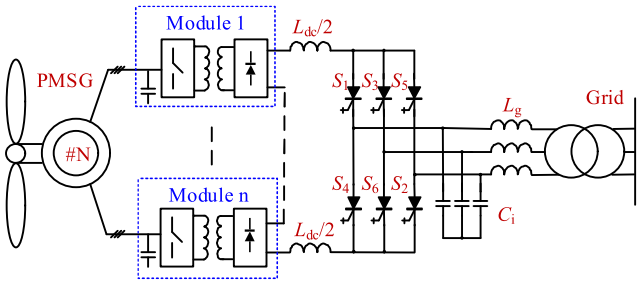

Fig. 2. Proposed modular DMC and CSC based WECS.

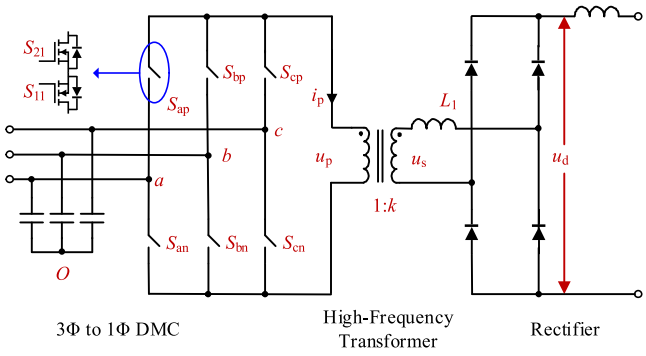

Fig. 3. Topology of DMC module.

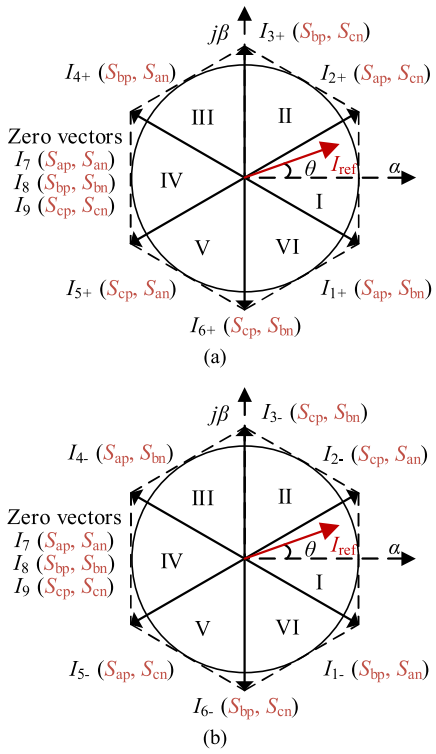

Fig. 4. Current vectors of DMC. (a) Positive part. (b) Negative part.

parts. The first part is the 3Φ to 1Φ DMC. Similar with CSI, the three-phase capacitors are used to help the commutation of power devices and filter the current harmonics in DMC. The bidirectional switches in DMC is realized by two single MOSFETs connected in common source pin. The second part is the high-frequency transformer, which provides the function of isolation for cascaded configuration of wind turbines in Figs. 1 and 2. The modular structure distributes the large capacity of wind turbine among several high-frequency transformers, which can facilitate convenient design of high-frequency transformers. The third part is the rectifier on the secondary side. In this article, the simple diode rectifier is used considering the power flow of WECS is unidirectional. Actually, the active rectifiers can be used to provide the bidirectional power ability [26].

III. Switching Modulation Strategy

As shown in Fig. 2, the current-source inverter (CSI) is applied on the grid side to regulate the dc-link current. There are already many pieces of literature on the switching modulation strategy for the CSC [16]–[18]. Hence, the operation principle of the grid-tied CSI is omitted. On the other hand, the switching modulation strategy of the proposed WECS will be investigated in detail as follows.

A. Space Vector Modulation

Generally, there are two types of DMC according to the dc-link of the passive rectifier [26]. In this article, the current-fed matrix converter is utilized in the proposed WECS to eliminate the use of electrolytic capacitors and provide the stable current for HVdc transmission. Based on the De-Re-Coupling idea in [36], the DMC is equivalent to the conventional CSC except the bidirectional power switches. Therefore, the modulation schemes for CSC can be applied in the DMC considering the current direction of the transformer. In this article, the space vector modulation (SVM) is used because of its fast dynamic performance and easy online implementation. Fig. 4 shows the current vector diagrams of the DMC. There are nine current vectors including six active vectors and three zero vectors in the conventional CSC. In the three-segment modulation, one zero vector and two adjacent active vectors are used to synthesize the reference vector by ampere-second balance principle. To generate ac voltage in the high-frequency transformer, the switching cycle of DMC is divided into two parts considering the polarity of transformer current. Fig. 4(a) shows the vector diagram when the transformer current i_p is positive while Fig. 4(b) shows the vector diagram when i_p is negative. As a matter of fact, the current vectors in Fig. 4 have opposite phases. For example, the current vector I_{1+} in Fig. 4(a) and I_{4-} in Fig. 4(b) have the same switching states. The dwell time calculation for the current vectors in one switching cycle has been proposed in [26].

In the conventional CSC, the sorting sequence of current vectors has been determined according to the principle of minimum switching actions and, thus, reduction of losses. Differently, the sorting sequence of vectors for DMC is determined by the output voltages for soft-switching operation of devices. Table I lists the switching states of current vectors and the corresponding output voltages, which indicates that the output voltages of DMC are determined by the switching states of current vectors. A comprehensive analysis of soft-switching operation with different switching patterns has been reported in [29]. It has been

TABLE I
SWITCHING STATES AND OUTPUT VOLTAGES OF DMC

Space vectors		Switching states	u_p
Active vectors	I_{1+} I_{4-}	S_{ap} S_{bn}	u_{ab}
	I_{2+} I_{5-}	S_{ap} S_{cn}	u_{ac}
	I_{3+} I_{6-}	S_{bp} S_{cn}	u_{bc}
	I_{4+} I_{1-}	S_{bp} S_{an}	$-u_{ab}$
	I_{5+} I_{2-}	S_{cp} S_{an}	$-u_{ac}$
	I_{6+} I_{3-}	S_{cp} S_{bn}	$-u_{bc}$
Zero vectors	I_7	S_{ap} S_{an}	0
	I_8	S_{bp} S_{bn}	
	I_9	S_{cp} S_{cn}	

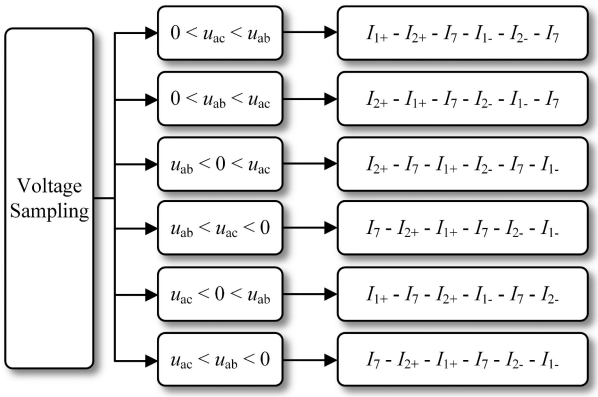

Fig. 5. Sorting algorithm of current vectors in Sector I.

concluded that the "Type A" PWM is ideal for the DMC because it can realize the zero-voltage switching (ZVS) for most of the power switches and have the least switching loss. To realize ZVS, the rising edges of the primary-side transformer voltage u_p should occur when the current i_p is negative, and vice versa. Different from the vector sorting algorithm method with the phase angle of power grid mentioned in [29], the sequence of current vectors is arranged with feedback of three-phase capacitor voltages in the proposed method. Therefore, the soft-switching operation can be guaranteed with different power factors for WECS. Fig. 5 shows the sorting algorithm of current vectors in Sector I, which is similar in other sectors.

B. Duty Loss Compensation

Fig. 6. shows the theoretical waveforms of the CF-HFT-MC in Sector I, where u_p and i_p are the primary-side voltage and current, respectively. The voltage u_d is the output voltage of the diode rectifier. i_{wa}, i_{wb}, and i_{wc} represent the three-phase input currents of the matrix converter, respectively. Assume that the magnitudes of three-phase capacitor voltages satisfy the condition $u_{ab} > u_{ac} > 0$, the sequence of current vectors is arranged as I_{1+} - I_{2+} - I_7 - I_{1-} - I_{2-} - I_7 according to the criterion in Fig. 5. The duty loss is caused by the commutation of the leakage inductor, which is unavoidable in the transformer. It happens

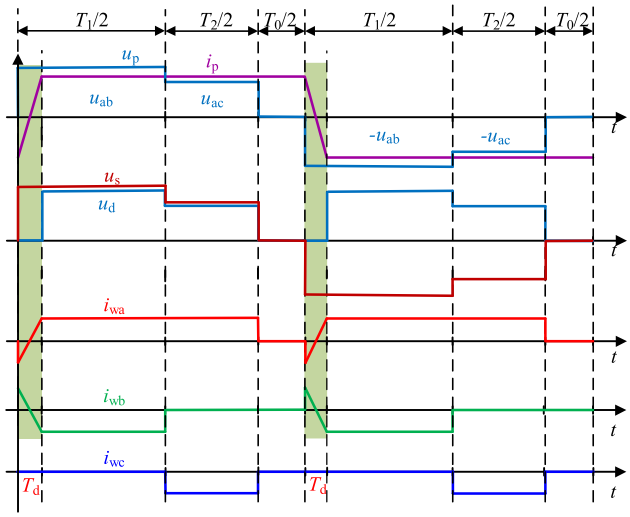

Fig. 6. Theoretical waveforms of DMC module in steady state.

at the transition moments from zero current vectors to active vectors. During the transition processes, the secondary-side voltage u_s of HFT is applied across the leakage inductor and the current of the leakage inductor changes the direction. The dc-link voltage u_d of the diode bridge rectifier is zero during this interval. Therefore, the duty cycle of u_d is less than that of the secondary-side voltage u_s of HFT. The areas of the duty loss have been shaded dark green in Fig. 6. As a result, the switching frequency is limited and the circulating current is generated in the CF-HFT-MC module. Moreover, additional harmonics are caused in the generator current by the duty loss because the dwell time of active current vectors is occupied. The period of duty loss T_d can be calculated by (1), where L_1, I_{dc} and k represent the leakage inductance value, the dc-link current and the turns ratio of the transformer, respectively. To reduce the current harmonics of the generator, the dwell time for each current vector can be recalculated in (2) to compensate the duty loss of active current vectors. T_s, m_r, and θ_r are the period of switching cycle, the modulation index, and the phase angel of the SVM, respectively. T_1, T_2, and T_0 are the time intervals for different current vectors in Sector I. Considering the duty loss occupies the dwell time of the first active vector, the compensation is presented for T_1. The calculation and compensation of intervals in other sectors are similar

$$T_d = 2L_1 I_{dc}/k u_{ab} \tag{1}$$

$$\begin{cases} T_1 = T_s m_r \sin(\pi/6 - \theta_r) + 2T_d \\ T_2 = T_s m_r \sin(\pi/6 + \theta_r) \\ T_0 = T_s - T_1 - T_2. \end{cases} \tag{2}$$

As aforementioned, there are two types of current vectors in the SVM of the CF-HFT-MC, i.e., the zero vectors and the active current vectors. When the zero current vectors work, the output voltage u_p of DMC is zero. There is no power transferred from the generator and the module to the grid. There are also two modes when the active current vectors work. One is the charging mode where the generator power is transferred to the

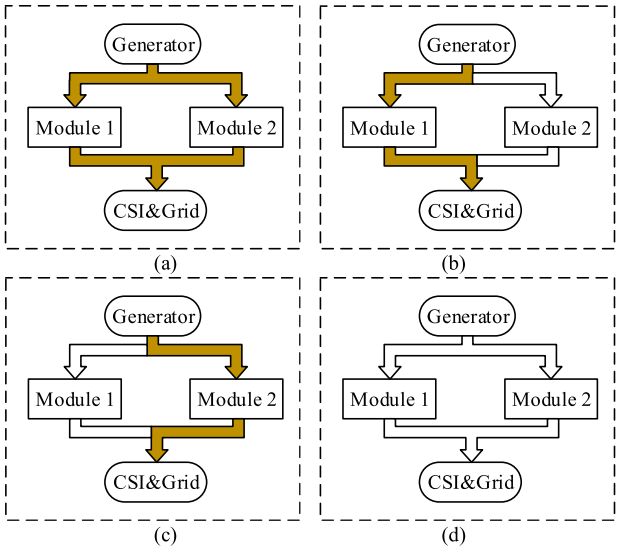

Fig. 7. Power flow diagrams of CF-HFT-DMC modules. (a) From both modules. (b) From module 1. (c) From module 2. (d) No power is transferred.

grid. The other mode is the freewheeling mode, which is caused by the duty loss. In this mode, the output voltage $u_{\rm p}$ keeps constant while the average value of $i_{\rm p}$ is zero. Hence, there is no power transferred in this mode. The power flow diagram of the freewheeling mode is the same as that of the zero current vector. As a result, there are totally four types of power flow diagram with two CF-HFT-MC modules in the experiment. Fig. 7 shows power flow diagrams of the two CF-HFT-MC modules under different conditions, where the solid arrows represent the active power flow transferring path and the hollow arrows represent no power transfer. The power is transferred from both module 1 and module 2 when the active current vectors work simultaneously, as shown in Fig. 7(a). Fig. 7(b) and (c) shows the power flow diagrams when the active power is transferred from a single module, i.e., module 1 or module 2, respectively. Fig. 7(d) shows the power flow diagram where no power is not transferred from these two modules.

C. Commutation

The bidirectional power switches in the CF-HFT-MC module are constructed by two single MOSFETs connected in common source pins in the proposed system. The commutation of the devices in the CF-HFT-MC module is critical because it affects the safe operation of the system. There are two constraints in the commutation process of CF-HFT-MC. The first one is that the upper or lower switches in different legs cannot be turned ON at the same time. Otherwise, the short-circuit faults will happen between the three-phase filter capacitors. Second, the path for the leakage inductor current cannot be interrupted. Otherwise, the voltage spikes will be excited and the power devices will be damaged. In this article, the four-step commutation method is utilized for safe operation. For the sake of brevity, the detailed process is omitted, which can be found in [26].

IV. Control Scheme of the Proposed WECS

The CF-HFT-MC is equivalent to conventional CSC according to the De-Re-Coupling idea in [36]. Therefore, the control scheme for the proposed modular CF-HFT-MC-based WECS is similar with that for back-to-back CSCs based WECS. Moreover, the cascaded configuration of the generators will not affect the maximum power point tracking (MPPT) of individual wind plant. In the proposed configuration, all wind turbines work with their own MPPT control method to capture the maximum wind power. The MPPT control for individual generator has been tested and verified in cascaded CSCs-based offshore wind farms in [21], which could also be applied to the proposed CF-HFT-MC-based WECS. However, the power sharing and balance of voltage and current among the CF-HFT-MC modules must be designed in control scheme for the proposed WECS. The other control targets of the proposed WECS include the generator-side active power control with MPPT, the dc-link current control, and the grid-side reactive power control. Fig. 8 shows the overall control diagram of the proposed IPOS CF-HFT-MC configuration. Both the modulation index and delay angle are used as the control variables for generator-side and grid-side converters.

A. Power Sharing and Voltage Balance Control

The MPPT is used for the control scheme on generator side to capture the maximum wind power at different wind speeds, which can be achieved by adjusting the turbine speed to realize the optimal tip speed ratio. In order to share the power evenly among CF-HFT-MC modules and avoid unbalance in voltage and current stresses, the power sharing and voltage balance control have to be achieved in the control scheme for CF-HFT-MC modules. As shown Fig. 8, all the CF-HFT-MC modules share the common delay angle $\alpha_{\rm r}$. Similar to CSCs, the *dq*-axis capacitor currents, namely $i_{\rm crd}$ and $i_{\rm crq}$ can be calculated by (3), where $\omega_{\rm r}$, $u_{\rm ds}$, $u_{\rm qs}$, and $C_{\rm r}$ represent the electric angular speed of permanent-magnet synchronous generator (PMSG), *dq*-axis terminal voltages and filter capacitors, respectively. The zero *d*-axis current control is utilized for the PMSG and the electric angle of the generator is obtained by the encoder

$$\begin{cases} i_{\rm crd} = -\omega_{\rm r} u_{\rm ds} C_{\rm r} \\ i_{\rm crq} = \omega_{\rm r} u_{\rm qs} C_{\rm r}. \end{cases} \tag{3}$$

If all the modular CF-HFT-MCs are with identical parameters ideally, the captured wind power can be evenly distributed among them. However, the parameters in the modular CF-HFT-MCs cannot be identical completely in practice. The parameters such as turns ratios of high-frequency transformers and the ON-state resistance of power devices will cause the unbalanced power distribution among CF-HFT-MC modules. The output dc terminals of modular CF-HFT-MCs are connected in series, and the diode bridges on the secondary-side of HFT share the common output current $I_{\rm d}$. Therefore, the unbalanced power distribution among CF-HFT-MC modules will cause unbalance in output voltages of CF-HFT-MCs. The balance of dc output voltage of CF-HFT-MC modules must be included in the control scheme.

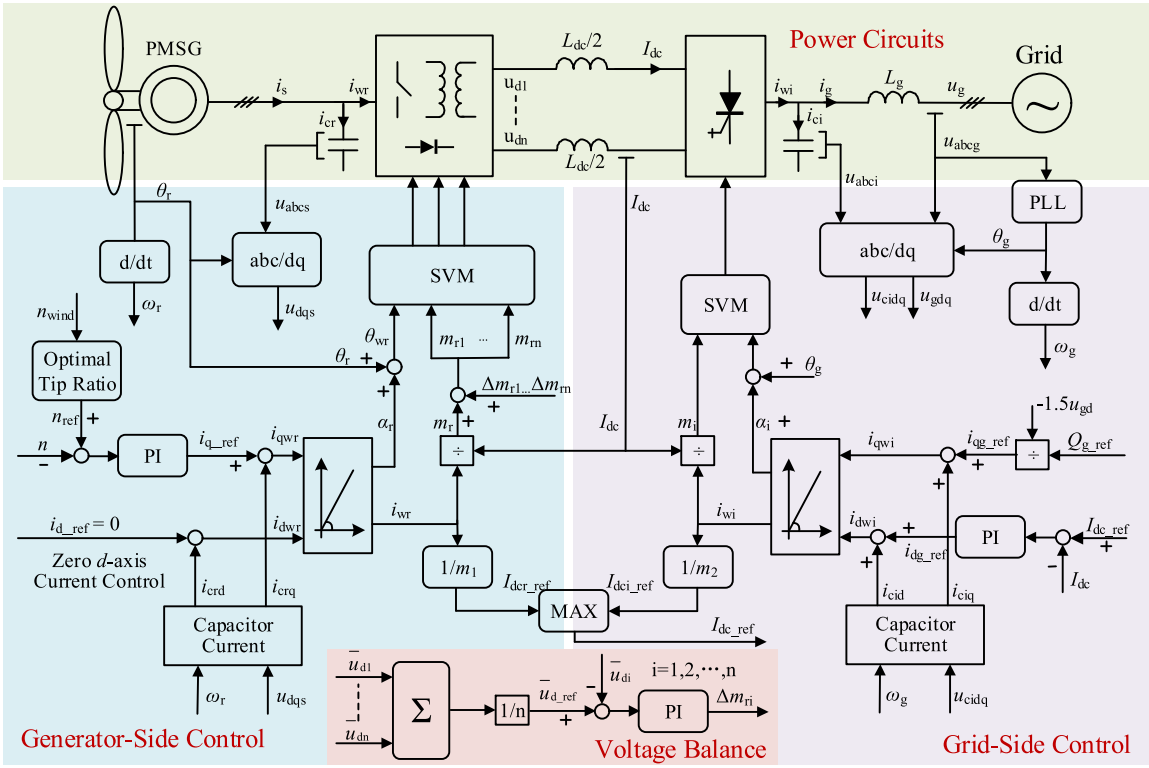

Fig. 8. Overall control diagram of the proposed configuration.

The power sharing of the WECS can be realized by the voltage balance control of the average dc-link voltages of the cascaded diode bridges. The average dc-link voltage of the current-source rectifier (CSR) can be calculated by (4), where $\overline{u}_{\rm d}$, $m_{\rm r}$ $v_{\rm LL}$ and α represent the average dc-link voltage, modulation index, line-to-line voltage of the filter capacitors, and the power factor. It indicates that the dc-link voltage is affected by the capacitor voltage, modulation index, and the power factor of CSR. In the proposed modular CF-HFT-MC-based WECS, all modules share the same capacitor voltages and common delay angle with the input parallel configuration on ac side. Hence, the modulation index of each CF-HFT-MC module can be utilized for voltage balance control of CF-HFT-MC, as shown in (5). Different from dc voltage of CSC in (4), the turns ratio of the transformer $k_{\rm i}$ also affects the dc output voltage of the HFT based MC module in (5).

As shown in Fig. 8, the average modulation index $m_{\rm r}$ is generated to control the total power of WECS, which provides the base value of modulation index for CF-HFT-MC modules in IPOS configuration. The average modulation index $m_{\rm r}$ is calculated according to the current reference $i_{\rm wr}$ and dc-link current $I_{\rm dc}$. Additionally, the individual part $\Delta m_{\rm r}$ is produced and added to the final modulation index as in (6) to achieve balance in dc output voltages and power sharing among CF-HFT-MC modules. For instance, the final modulation index $m_{\rm r1}$ for the first CF-HFT-MC module is composed of the average $m_{\rm r}$ and the individual $\Delta m_{\rm r1}$

$$\overline{u}_{\rm d} = \sqrt{\frac{3}{2}} m_{\rm r} v_{\rm LL} \cos\alpha \tag{4}$$

$$\overline{u}_{\rm di} = \sqrt{\frac{3}{2}} m_{\rm ri} v_{\rm LL} k_{\rm i} \cos\alpha, {\rm i} = 1, 2, \ldots, {\rm n} \tag{5}$$

$$m_{\rm ri} = m_{\rm r} + \Delta m_{\rm ri}, {\rm i} = 1, 2, \ldots, {\rm n}. \tag{6}$$

The generation of additional parts of modulation index $\Delta m_{\rm r}$ is given in Fig. 8. The proportion–integration (PI) controllers are used to make the dc output voltage track the average value of the total dc-link voltage. In such away, the even power distribution can be achieved with the equal average dc-link voltages of CF-HFT-MC modules.

B. DC-Link Current Regulation

Different from the constant dc-link voltage of voltage-source converters, the dc-link voltage of CSC varies according to the grid voltages and switching states. The dc-link current plays a critical role in the CSC based WECSs as it determines the efficiency and the dynamic performance of the system. The fixed dc-link current can provide a fast dynamic performance, but the conduction loss is high in the power devices and the dc choke. On the other hand, the change of dc-link current with variation of wind power can minimize the conduction loss and improve the efficiency of system. But the dynamic performance of the system will be limited by the current change in dc link. For WECS, the dynamic performance is not as important as the system efficiency as the wind power changes not fast. To obtain higher efficiency in the CSC-based wind farms, the dc-link current is varied according to the output power of the generator in the

proposed WECS

$$\begin{cases} i_{\rm cid} = -\omega_{\rm g} u_{\rm cid} C_{\rm i} \\ i_{\rm ciq} = \omega_{\rm g} u_{\rm ciq} C_{\rm i}. \end{cases} \tag{7}$$

For the sake of brevity, the conventional method of dc-link current control for the CSC based WECS is utilized in this system [2]. The final dc-link current reference $I_{\rm dc\_ref}$ is selected from the dc-link current reference both from the modular DMC on generator side and the CSI on grid side, i.e., $i_{\rm wr}$ and $i_{\rm wi}$. m_1 and m_2 are the maximum average modulation index of CF-HFT-MC modules and CSI, respectively. Both of them are set as 0.9 in the proposed system. Therefore, the individual part $\Delta m_{\rm r}$ is limited within (–0.1, 0.1) to avoid the saturation of the final modulation index $m_{\rm ri}$ for each CF-HFT-MC module. As shown in Fig. 8, the higher value of $I_{\rm dcr\_ref}$ and $I_{\rm dci\_ref}$ will be selected as the final $I_{\rm dc\_ref}$ for dc-link current reference.

Different from the generator-side control, the angle $\theta_{\rm g}$ and electric angular speed $\omega_{\rm g}$ of the grid is obtained by the phase locked loop. The capacitor currents $i_{\rm cid}$ and $i_{\rm ciq}$ are compensated by (7) where $u_{\rm cid}$, $u_{\rm ciq}$, and $C_{\rm i}$ represent the dq-axis terminal voltage and filter capacitors. The reactive power is controlled by the q-axis current reference $i_{\rm qg\_ref}$ and the d-axis current reference $i_{\rm dg\_ref}$ is determined by the closed-loop control of dc-link current.

V. Simulations and Experiments

The performance of the proposed modular CF-HFT-MC-based WECS has been verified by both simulations and experiments. The MATLAB/Simulink is used to conduct simulation on a 1 MW/690 V PMSG-based WECS, which is integrated to the 3300 V-grid through 4 CF-HFT-MC modules in IPOS configuration. For experiments, the low-power prototype of PMSG-based WECS is built for verification due to the limited power conditions in lab. The parameters of grid, PMSG, CF-HFT-MC modules, and CSI in simulations and experiments are presented in Table II.

A. Simulation

First, the simulation is carried out with four CF-HFT-MC modules in the WECS. To verify the performance of the power sharing and voltage balance, the turns ratio of the four medium frequency transformers has been set different. The turns ratios of transformers of module 1 and module 2 are 1:1, while turns ratios of transformers are 1:1.1 in module 3 and module 4. Therefore, the output voltages of module 3 and module 4 will be higher than those of module 1 and module 2, as shown in Fig. 9. With the compensation of the modulation index, the output voltages of different modules are balanced well. Moreover, it can be observed that the additional PI regulators do not affect the dc-link current $I_{\rm dc}$ at steady state. Fig. 10 shows the dynamic voltage balance performance and the MPPT operation under change of wind speed. The reference speed $n_{\rm ref}$ is generated from the optimal tip ratio method of MPPT and the actual rotor speed n tracks the reference well. The output power of the generator responds quickly to the vibrations of the speed. When the speed reference decreased to 0.8 p.u., the output power reduced to 0.51 p.u. with the optimal tip ratio method. The voltage balance control is not affected by the change of wind speed.

The fault-tolerant operation capability is crucial for system safety of WECS. There already exist several research works on modulation and control schemes of the CSIs under grid faults [37], which are still suitable for onshore inverters in this article. On the other hand, when one power switch is faulty in one CF-HFT-MC module, the other switches in the same module will be turned OFF. Then, the corresponding part on

TABLE II
Parameters of the System

Parameters	Simulation	Experiment
Grid Side		
Nominal Power	1 MW	1 kW
Grid Voltage	3300 V (rms)	150 V (rms)
Frequency	50 Hz	50 Hz
PMSG Side		
Nominal Voltage	690 V (rms)	70 V (rms)
Synchronous Inductance	1.57 mH	1.47 mH
Number of Poles	26	4
Rated Speed	25 RPM	1000 RPM
CF-HFT-MC Module		
Number of Modules	4	2
Turns Ratio	1:1 (Module 1-2) 1:1.1 (Module 3-4)	1:1, 1:1 Tolerance ±2%
Filter Capacitor	4*100 μF	2*9.4 μF
Switching Frequency	20 kHz	20 kHz
Sample Time	50 μs	50 μs
CSI		
DC-link Inductor	30 mH	6 mH
Filter Capacitor	100 μF	30 μF
Filter Inductor	10 mH	5 mH
Switching Frequency	5 kHz	5 kHz
Sample Time	200 μs	200 μs
Modulation Scheme	SVM	SVM

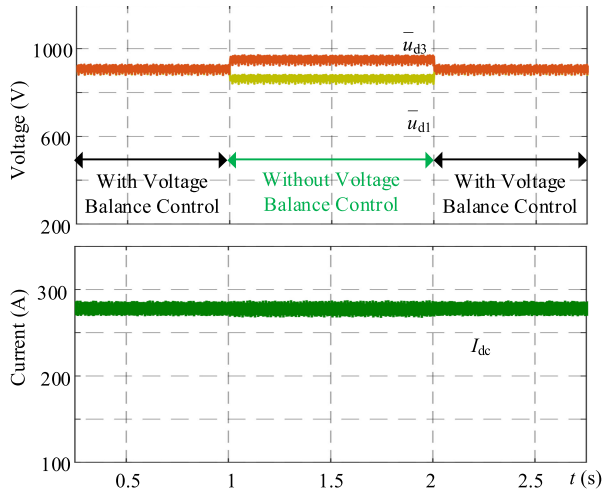

Fig. 9. Simulation results at steady state including the average output voltage of DMC modules and the dc-link current $I_{\rm dc}$.

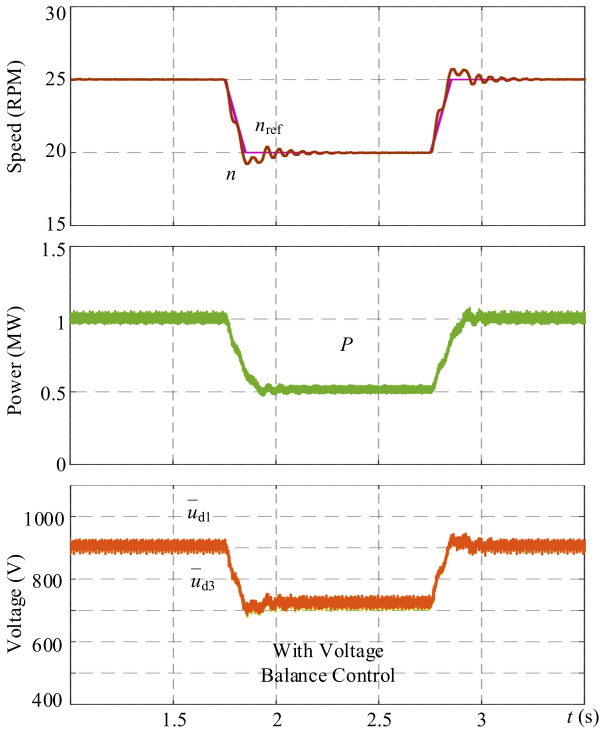

Fig. 10. Simulation results under change of wind speed including the speed reference n_{ref}, the output power P, the actual rotor speed n, and the average output voltage of DMC modules.

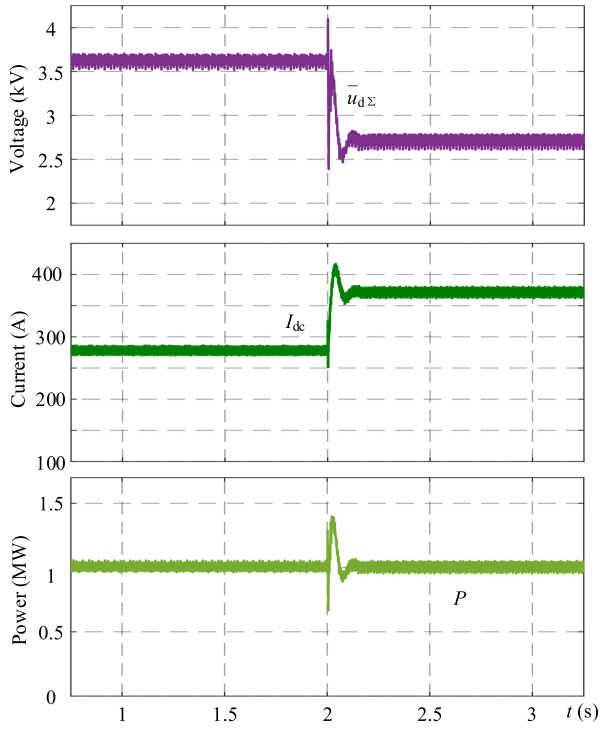

Fig. 11. Simulation results of fault-tolerant operation of WECS when module 4 is faulty, including the total output voltage of modular HFT-MC $\overline{u}_{\mathrm{d}\Sigma}$, the dc-link current I_{dc}, and the output power P.

primary-side of CF-HFT-MC module could be isolated from the system. However, the diode bridge on the secondary side of CF-HFT-MC module could still provide the current path for the dc-link current. Consequently, the dc-link current will not be interrupted, which is essential for fault-tolerant operation of the whole system. Fig. 11 shows the simulated results of the proposed system under fault condition. Before t = 2s, four modules work under normal condition. When t = 2s, module 4 is faulty and isolated from the system by removing all the driving signals. As a result, the total average output voltage $\overline{u}_{\mathrm{d}\Sigma}$ is reduced due to removal of module 4. The dc-link current I_{dc} increases accordingly to ensure the same active power transferring.

B. Experiments

A low-power laboratory prototype has been built to verify the effectiveness of the proposed CF-HFT-MC-based WECS. Two MC modules are constructed in the system. Fig. 12 shows the photograph of experimental setup. The power devices are 650 V CoolMOS (IPZ65R095C7) from Infineon both for HFT-MC on generator side and CSI on grid side. The diodes used in the secondary-side H-bridge and the CSI are MUR3060WT designed by ON Semiconductor. Two digital signal processors (DSPs) are used in the system to simulate the onshore and offshore control schemes: One is for implementing control algorithm and generating switching pulses for the modular CF-HFT-MC, and the other is for CSI. The two CF-HFT-MC modules are controlled with one single DSP. If more modules

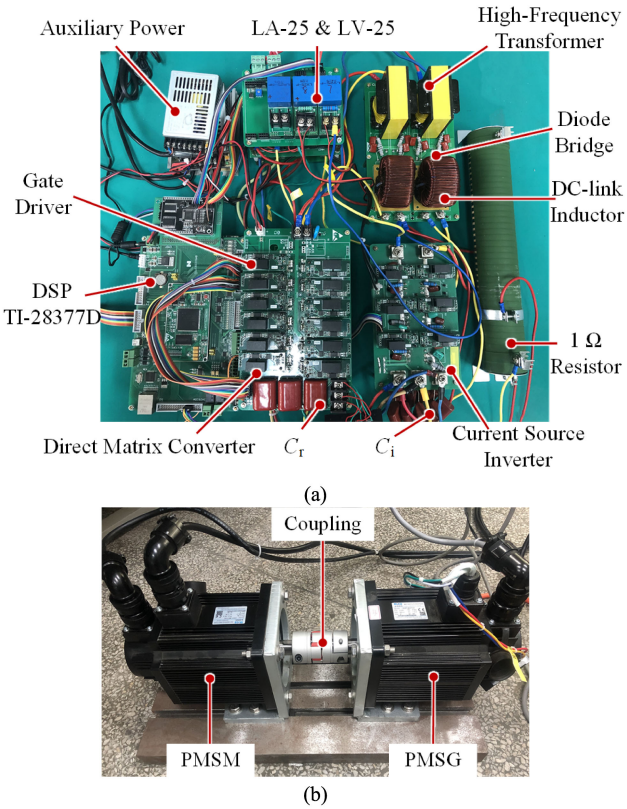

Fig. 12. Photograph of the experimental setup. (a) CF-HFT-MC modules and CSI. (b) Mechanically coupled PMSM and PMSG.

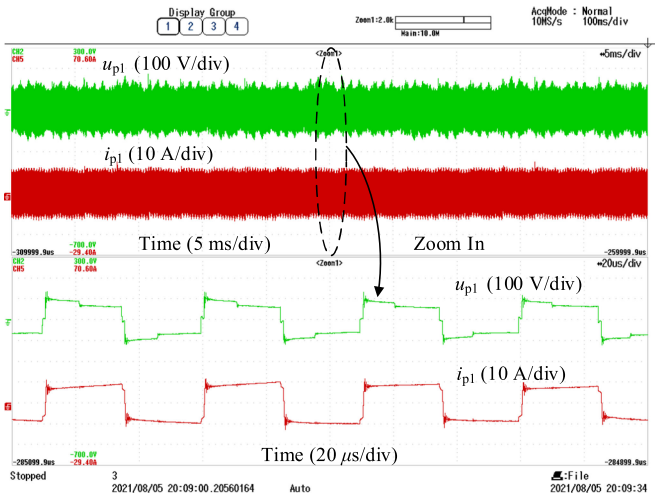

Fig. 13. Output voltage u_{p1} and current i_{p1} of module 1.

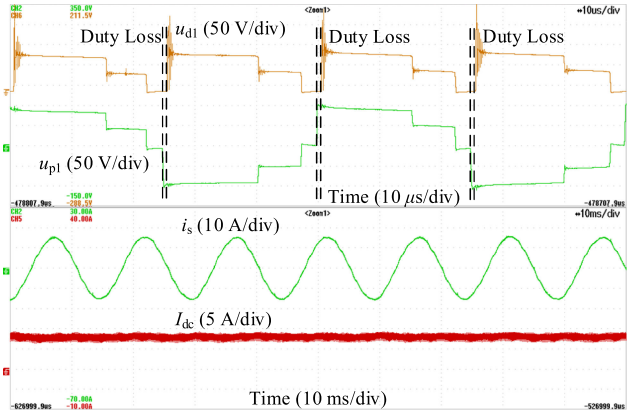

Fig. 14. Duty loss and the measured currents of the converter.

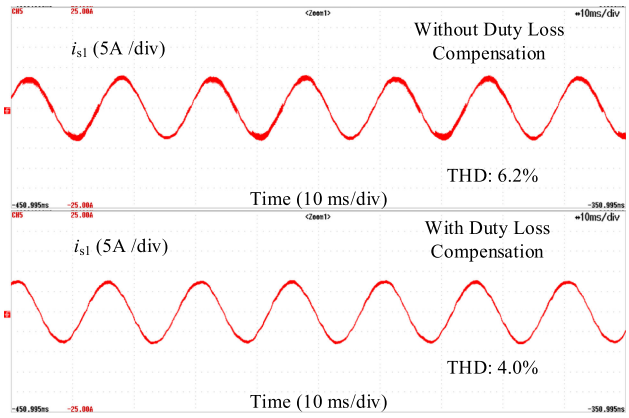

Fig. 15. THD comparison of phase current w/o the duty loss compensation.

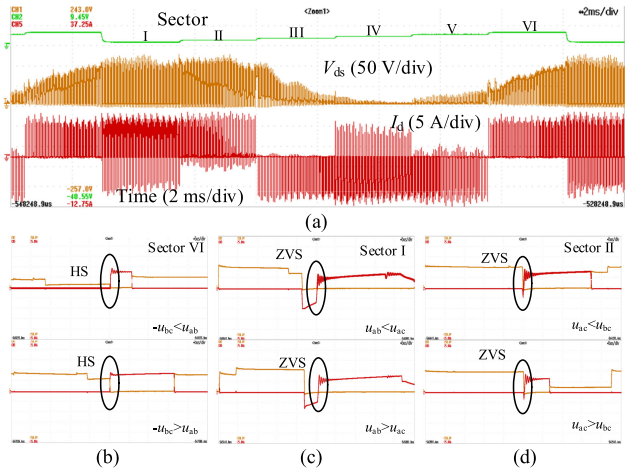

Fig. 16. Drain–source voltage V_{ds} (50 V/div) and current I_d (5 A/div) of switch S_{11} in module 1 with different sectors and three-phase capacitor voltages. (a) I_d, V_{ds} and sector of SVM. (b)–(d) Zoomed waveforms of I_d and V_{ds} in Sectors VI, I and II, respectively (X: 5 μs/div).

are needed in the system, the field-programmable gate array can be used. One PMSG works as the wind power generator, which is coupled mechanically to a permanent-magnet synchronous motor (PMSM). The speed of PMSG is controlled by the CF-HFT-MC modules, as shown in Fig. 8. The PMSM is used to provide torque for the PMSG, and the PMSM is controlled to output a desired electromagnetic torque by a commercial power inverter.

Fig. 13 shows the measured steady-state primary-side current i_{p1} and voltage u_{p1} of module 1. With the sorting algorithm in Fig. 5, the voltage u_{p1} steps down at each half switching cycle, which implies that the ZVS is achieved during the switching transients. Fig. 14 shows the duty loss, the phase current of the generator i_s and the dc-link current I_{dc}. As the commutation of the leakage inductor (10 μH in the experiment) cannot be finished instantly, the duty loss of the CF-HFT-MC is hard to be mitigated. The commutation occupies the dwell time of active current vectors, which will increase the current harmonics. As a result, the compensation of duty loss is conducted in this article. Fig. 15 shows the comparison of the phase current i_{s1} with and without duty loss compensation. It indicates the low-order harmonics of the system is reduced and the total harmonic distortion (THD) of the system decreases from 6.2% to 4.0% with the duty loss compensation.

With the four-step commutation, a current path is always provided for the leakage inductor of HFT. Consequently, the voltage spikes are eliminated for the power switches in CF-HFT-MC modules. The additional clamp circuits are not required in the proposed WECS. Fig. 16(a) shows the drain–source voltage V_{ds} and current I_d of switch S_{11} in module 1. It can be observed that there is no high voltage spike in the experiment. Furthermore, the current I_d in Sector III and Sector V is zero or -I_{dc}, which means that the synchronous rectification is realized for the switch S_{11}. Therefore, ZVS is achieved in Sectors III and V. As shown in Fig. 16(a), the drain–source voltage V_{ds} is zero in Sector IV, which implies that the soft-switching is also realized in Section IV. The detailed waveforms of V_{ds} and I_d of S_{11} in Sectors VI, I, and II are shown in Fig. 16(b)–(d), respectively. It can be found that the soft-switching is realized in Sectors I and II while the hard-switching is presented in Sector VI. The switching conditions of other switches in CF-HFT-MC modules are similar to that of S_{11}. As a result, the proposed modulation

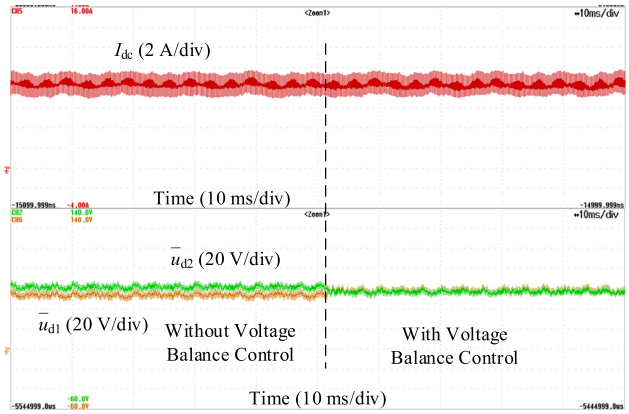

Fig. 17. Voltage balance and the dc-link current I_{dc}.

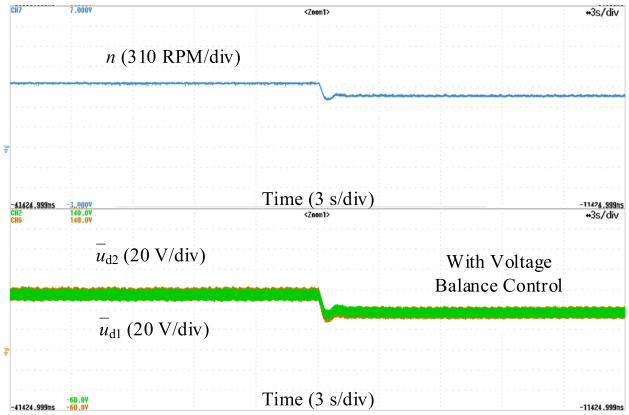

Fig. 18. Performance of voltage balance during change of speed.

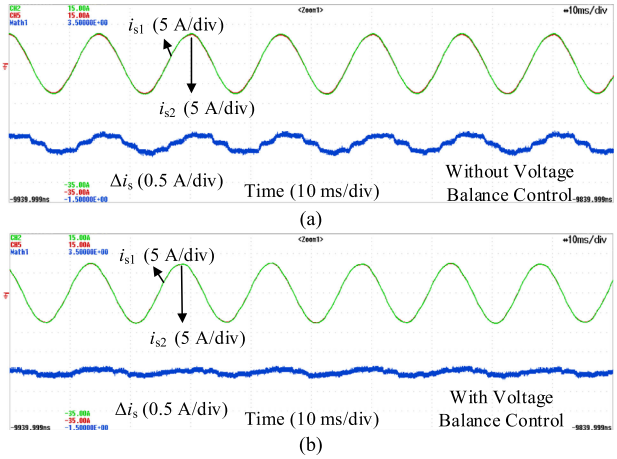

Fig. 19. Input currents of module 1 and module 2 and the current difference Δi_s. (a) Without voltage balance control. (b) With voltage balance control.

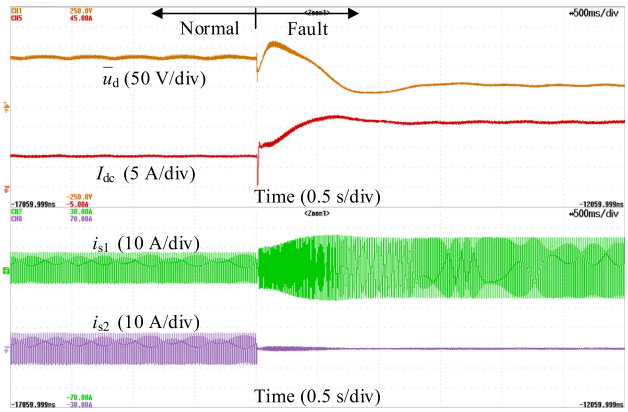

Fig. 20. Measured waveforms under fault of module 2.

method realizes soft-switching for most of the power devices with the sorting algorithm method shown in Fig. 5.

Moreover, the power sharing and voltage balance performance is verified in the experiment. The nominal turns ratio in both the two transformers in DMC is 1:1. To stimulate the unbalance, a 1-Ω resistor is connected in series with the diode rectifier of module 2 purposely. Fig. 17 shows the detailed waveforms of the average output voltage $\overline{u}_{d1}$ and $\overline{u}_{d2}$ of the two HFT-MC modules. With the additional resistor, the average output voltage of module 2 is higher without voltage balance. On the other hand, the average output voltages of the modules are controlled equal with the proposed voltage balance method. The average output voltage of CF-HFT-MC modules is measured with a first-order low-pass filter. The dc-link current keeps constant during the transition between different methods. Additionally, the performance of voltage balance is not affected during change of speed, as shown in Fig. 18. Therefore, it is verified that the proposed voltage balance method is effective for both steady state and dynamic state. Additionally, an additional 2-μH leakage inductor is added purposely between DMC and HFT in module 2 to increase the unbalance in system and clarify the effectiveness of power balancing. Fig. 19 shows the measured input currents i_{s1} and i_{s2} for module 1 and module 2, respectively. Moreover, the difference between them Δi_s ($i_{s1} - i_{s2}$) is also calculated and displayed by the oscilloscope. Due to the additional leakage inductor, the duty loss of module 2 is larger than module 1, which results in a lower transferring power with the same dc-link current. Hence, the amplitude of input current of module 1 is higher than that of module 2. The amplitude of the difference Δi_s is about 0.3 A, as shown in Fig. 19(a). However, with the load sharing method, the amplitude of Δi_s reduces dramatically to about 0.1 A, as shown in Fig. 19(b).

The modular design of the proposed configuration increases the reliability of the WECS. When the fault occurs in the DMC, the faulty module will be isolated from the system. However, the secondary-side diode bridge rectifier of the faulty module provides the current path for the dc-link inductor. The left healthy modules can still carry the power form the generator. Fig. 20 shows the experimental performance of the modular CF-HFT-MC modules under the fault condition. Suppose that the fault happens in module 2 and it is isolated from the CF-HFT-MC-based WECS. The input current i_{s2} of module 2 reduces to zero and the total average output voltage $\overline{u}_d$ reduces to the half of the rated value. The dc-link current I_{dc} and the input current i_{s1} of module 1 rises accordingly to keep the same output power. Fig. 21 shows the experimental waveforms of the grid current i_{ga} and voltage u_{ga} of phase a. It verifies that the proposed WECS

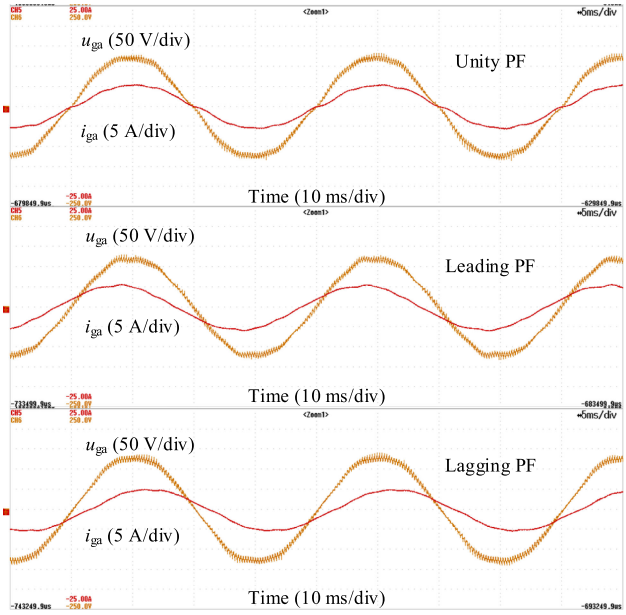

Fig. 21. Grid voltage u_{ga} and current i_{ga} under different PF conditions.

could operate under different power factors on grid side. Both the leading PF and the lagging PF are 0.9 in the experiments.

VI. Conclusion

In this article, a modular CF-HFT-MC-based cascaded configuration is proposed for off-shore WECS. The advantages of the proposed WECS system can be summarized as follows. First, the use of electrolytic capacitors is avoided completely in the CF-HFT-MC modules, and the reliability and service life of the converter can be improved. Second, the single-stage conversion and soft-switching are achieved for the CF-HFT-MC, which can help increase the efficiency of the system. Third, the dedicated modulation strategy and control scheme have been proposed for the CF-HFT-MC-based WECS system, where the IPOS connection is employed to integrate the low-voltage wind turbines into the HVdc transmission system. Not only the safe commutation is provided for the CF-HFT-MC but also even power distribution and balanced output voltage are achieved for multiple power modules. Both the simulations and laboratory experiments have been conducted to verify the effectiveness of the proposed system.

References

[1] V. Yaramasu, B. Wu, P. C. Sen, S. Kouro, and M. Narimani, "High-power wind energy conversion systems: State-of-the-art and emerging technologies," *Proc. IEEE*, vol. 103, no. 5, pp. 740–788, May 2015.

[2] B. Wu, Y. Lang, N. Zargari, and S. Kouro, *Power Conversion Control Wind Energy Systems*. New York, NY, USA: Wiley, 2011.

[3] C. Chou, Y. Wu, G. Han, and C. Lee, "Comparative evaluation of the HVDC and HVAC links integrated in a large offshore wind farm—An actual case study in taiwan," *IEEE Trans. Ind. Appl.*, vol. 48, no. 5, pp. 1639–1648, Sep./Oct. 2012.

[4] B. Gustavsen and O. Mo, "Variable transmission voltage for loss minimization in long offshore wind farm AC export cables," *IEEE Trans. Power Del.*, vol. 32, no. 3, pp. 1422–1431, Jun. 2017.

[5] "Offshore wind connections," Accessed: Sep. 2017. [Online]. Available: http://new.abb.com/systems/offshore-wind-connections

[6] M. Guan, "A series-connected offshore wind farm based on modular dual-active-bridge (DAB) isolated DC–DC converter," *IEEE Trans. Energy Convers.*, vol. 34, no. 3, pp. 1422–1431, Sep. 2019.

[7] G. P. Adam *et al.*, "Improved two-level voltage source converter for high-voltage direct current transmission systems," *IEEE J. Emerg. Sel. Topics Power Electron.*, vol. 5, no. 4, pp. 1670–1686, Dec. 2017.

[8] M. Gu, Z. Wang, K. Yu, X. Wang, and M. Cheng, "Interleaved model predictive control for three-level neutral point clamped dual three-phsae PMSM drives with low switching frequencies," *IEEE Trans. Power Electron.*, vol. 36, no. 10, pp. 11618–11630, Oct. 2021.

[9] G. Liu, F. Xu, Z. Xu, Z. Zhang, and G. Tang, "Assembly HVDC breaker for HVDC grids with modular multilevel converters," *IEEE Trans. Power Electron.*, vol. 32, no. 2, pp. 931–941, Feb. 2017.

[10] H. Wang *et al.*, "Lifetime estimation of DC-link capacitors in adjustable speed drives under grid voltage unbalances," *IEEE Trans. Power Electron.*, vol. 34, no. 5, pp. 4064–4078, May 2019.

[11] P. Liu, Z. Wang, Y. Xu, H. Xiao, and Y. Li, "Optimal overlap-time distribution of space vector modulation for current-source rectifier," *IEEE Trans. Ind. Electron.*, vol. 68, no. 6, pp. 4586–4597, Apr. 2021.

[12] P. Liu, Z. Wang, Y. Xu, Z. Zou, F. Deng, and Y. Li, "Improved harmonic profile for high-power PWM current-source converters with modified space vector modulation," *IEEE Trans. Power Electron.*, vol. 36, no. 10, pp. 11234–11244, Oct. 2021.

[13] Z. Wang, B. Wu, D. Xu, and N. R. Zargari, "A current-source-converter-based high-power high-speed PMSM drive with 420-Hz switching frequency," *IEEE Trans. Ind. Electron.*, vol. 59, no. 7, pp. 2970–2981, Jul. 2012.

[14] Z. Wang, Y. Xu, P. Liu, Y. Zhang, and J. He, "Zero-voltage-switching current source inverter fed PMSM drives with reduced EMI," *IEEE Trans. Power Electron.*, vol. 36, no. 1, pp. 761–771, Jan. 2021.

[15] Y. Xu, Z. Wang, P. Liu, and J. He, "A soft-switching current-source-inverter-fed motor drive with reduced common-mode voltage," *IEEE Trans. Ind. Electron.*, vol. 68, no. 4, pp. 3012–3021, Apr. 2021.

[16] R. A. Torres, H. Dai, T. M. Jahns, and B. Sarlioglu, "Operation Anal. Curr.-source inverters using dual-gate four-quadrant wide-bandgap power switches," in *Proc. IEEE Energy Convers. Congr. Expo.*, Baltimore, MD, USA, 2019, pp. 2353–2360.

[17] M. Guacci *et al.*, "Three-phase two-third-PWM buck-boost current source inverter system employing dual-gate monolithic bidirectional GaN e-FETs," *CPSS Trans. Power Electron. Appl.*, vol. 4, no. 4, pp. 339–354, Dec. 2019.

[18] O. E. Oni, I. E. Davidson, and K. N. I. Mbangula, "A review of LCC-HVDC and VSC-HVDC technologies and applications," in *Proc. IEEE 16th Int. Conf. Environ. Elect. Eng.*, Florence, Italy, 2016, pp. 1–7.

[19] Z. Wang, Y. Zheng, M. Cheng, and S. Fan, "Unified control for a wind turbine-superconducting magnetic energy storage hybrid system based on current source converters," *IEEE Trans. Magn.*, vol. 48, no. 11, pp. 3973–3976, Oct. 2012.

[20] J. Dai, D. Xu, and B. Wu, "A novel control scheme for current-source-converter-based PMSG wind energy conversion systems," *IEEE Trans. Power Electron.*, vol. 24, no. 4, pp. 963–972, Apr. 2009.

[21] M. Popat, B. Wu, F. Liu, and N. Zargari, "Coordinated control of cascaded current-source converter based offshore wind farm," *IEEE Trans. Sustain. Energy*, vol. 3, no. 3, pp. 557–565, Jul. 2012.

[22] Y. Xia, K. H. Ahmed, and B. W. Williams, "A PWM current source-based DC transmission system for multiple wind turbine interfacing," *IEEE J. Emerg. Sel. Topics Power Electron.*, vol. 2, no. 4, pp. 784–796, Dec. 2014.

[23] H. Chen and D. Divan, "Soft-switching solid-state transformer (S4T)," *IEEE Trans. Power Electron.*, vol. 33, no. 4, pp. 2933–2947, Apr. 2018.

[24] Q. Wei, B. Wu, D. Xu, and N. R. Zargari, "A medium-frequency transformer-based wind energy conversion system used for current-source converter-based offshore wind farm," *IEEE Trans. Power Electron.*, vol. 32, no. 1, pp. 248–259, Jan. 2017.

[25] Q. Wei, B. Wu, D. Xu, and N. R. Zargari, "A new configuration using PWM current source converters in low-voltage turbine-based wind energy conversion systems," *IEEE J. Emerg. Sel. Topics Power Electron.*, vol. 6, no. 2, pp. 919–929, Jun. 2018.

[26] Y. Xu, Z. Wang, P. Liu, Z. -X. Zou, and H. Xiao, "Current-fed isolated three-phase matrix-type grid inverter with soft-switching capability," *IEEE Trans. Ind. Electron.*, to be published, doi: 10.1109/TIE.2021.30733 06.

[27] D. Varajão, R. E. Araújo, L. M. Miranda, and J. A. P. Lopes, "Modulation strategy for a single-stage bidirectional and isolated AC–DC matrix converter for energy storage systems," *IEEE Trans. Ind. Electron.*, vol. 65, no. 4, pp. 3458–3468, Apr. 2018.

[28] L. Guan, Z. Wang, P. Liu, and J. Wu, "A three-phase to single-phase matrix converter for bidirectional wireless power transfer system," in *Proc. 45th Annu. Conf. IEEE Ind. Electron. Soc.*, Lisbon, Portugal, 2019, pp. 4451–4456.
[29] J. Afsharian, D. Xu, B. Wu, B. Gong, and Z. Yang, "The optimal PWM modulation and commutation scheme for a three-phase isolated buck matrix-type rectifier," *IEEE Trans. Power Electron.*, vol. 33, no. 1, pp. 110–124, Jan. 2018.
[30] A. Garcés and M. Molinas, "A study of efficiency in a reduced matrix converter for offshore wind farms," *IEEE Trans. Ind. Electron.*, vol. 59, no. 1, pp. 184–193, Jan. 2012.
[31] S. Peyghami, F. Blaabjerg, and P. Palensky, "Incorporating power electronic converters reliability into modern power system reliability analysis," *IEEE J. Emerg. Sel. Topics Power Electron.*, vol. 9, no. 2, pp. 1668–1681, Apr. 2021.
[32] T. M. Jahns and B. Sarlioglu, "The incredible shrinking motor drive: Accelerating the transition to integrated motor drives," *IEEE Power Electron Mag*, vol. 7, no. 3, pp. 18–27, Sep. 2020.
[33] H. Liu, M. S. A. Dahidah, J. Yu, R. T. Naayagi, and M. Armstrong, "Design and control of unidirectional DC–DC modular multilevel converter for offshore DC collection point: Theoretical analysis and experimental validation," *IEEE Trans. Power Electron.*, vol. 34, no. 6, pp. 5191–5208, Jun. 2019.
[34] J. E. Huber and J. W. Kolar, "Applicability of solid-state transformers in today's and future distribution grids," *IEEE Trans. Smart Grid*, vol. 10, no. 1, pp. 317–326, Jan. 2019.
[35] D. Zhou, Y. Song, Y. Liu, and F. Blaabjerg, "Mission profile based reliability evaluation of capacitor banks in wind power converters," *IEEE Trans. Power Electron.*, vol. 34, no. 5, pp. 4665–4677, May 2019.
[36] Z. Yan, K. Zhang, J. Li, and W. Wu, "A novel absolute value logic SPWM control strategy based on de-re-coupling idea for high frequency link matrix rectifier," *IEEE Trans. Ind. Informat.*, vol. 9, no. 2, pp. 1188–1198, May 2013.
[37] Y. Xu, Z. Wang, C. Li, and J. He, "Common-mode voltage reduction and fault-tolerant operation of four-leg CSI fed motor drives," *IEEE Trans. Power Electron.*, vol. 36, no. 8, pp. 8570–8574, Aug. 2021.

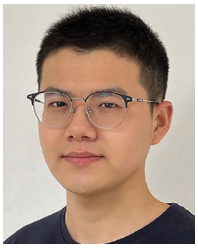

Yang Xu (Student Member, IEEE) received the B.Sc. degree in electrical engineering in 2018 from Southeast University, Nanjing, China, where he is currently working toward the Ph.D. degree in electrical engineering from the School of Electrical Engineering.

His research interests include current-fed high frequency converters, wide-bandgap device applications, and motor drives.

Zheng Wang (Senior Member, IEEE) received the B.Eng. and M.Eng. degrees from Southeast University, Nanjing, China, in 2000 and 2003, respectively, and the Ph.D. degree from the University of Hong Kong, Hong Kong, in 2008, all in electrical engineering.

From 2008 to 2009, he was a Postdoctoral Fellow with Ryerson University, Toronto, ON, Canada. He is currently a Full Professor with the School of Electrical Engineering, Southeast University. He has authored more than 120 internationally refereed papers, 1 English book by IEEE-Wiley Press, and 2 English book chapters on the topics of his research interests, which include electric drives, power electronics, and distributed generation.

Prof. Wang was a recipient of the IEEE PES Chapter Outstanding Engineer Award, First-class Science and Technology Award of Jiangsu Province in China, and Outstanding Young Scholar Award of Jiangsu Natural Science Foundation of China. He is an IET Fellow and an Associate Editor for the IEEE TRANSACTIONS ON INDUSTRIAL ELECTRONICS.

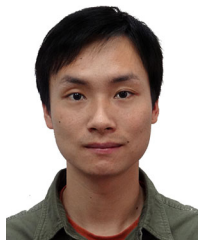

Pengcheng Liu (Student Member, IEEE) received the B.Sc. degree in electrical engineering in 2016 from Southeast University, Nanjing, China, where he is currently working toward the Ph.D. degree in electrical engineering with the School of Electrical Engineering.

His research interests include current-source converter, modulation techniques, motor drives, and renewable energy generation.

Qiang Wei received the B.Sc. degree from the Henan University of Science and Technology, Luoyang, China, in 2008, the M.A.Sc. degree from Xi'an Jiaotong University, Xi'an, China, in 2012, and the Ph.D. degree from Ryerson University, Toronto, ON, Canada, in 2017, all in electrical engineering.

From 2012 to 2014, he was with Delta Power Electronics, Nanjing, China, as an R&D Engineer. In 2018, he was with Lakehead University, Ontario, Canada, where he is currently an Assistant Professor. His research interests include innovative power conversions and controls for high power applications, such as renewable energies, drives, and electric vehicles.

Fujin Deng (Senior Member, IEEE) received the B. Eng. degree in electrical engineering from the China University of Mining and Technology, Jiangsu, China, in 2005, the M.Sc. degree in electrical engineering from Shanghai Jiao Tong University, Shanghai, China, in 2008, and the Ph.D. degree in energy technology from the Department of Energy Technology, Aalborg University, Aalborg, Denmark, in 2012.

He was with Southeast University in 2017 as a Professor with the School of Electrical Engineering, Southeast University, Nanjing, China. From 2013 to 2015 and from 2015 to 2017, he was a Postdoctoral Researcher and an Assistant Professor, respectively, with the Department of Energy Technology, Aalborg University. His main research interests include wind power generation, multilevel converters, high-voltage direct-current technology, dc grid, and offshore wind farm-power systems dynamics.

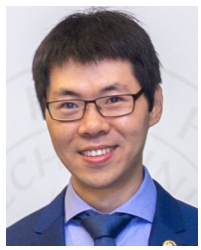

Zhixiang Zou (Senior Member, IEEE) received the B.Eng. and Ph.D. degrees in electrical and engineering from Southeast University, Nanjing, China, in 2007 and 2014, respectively, and the Dr.-Ing. degree (*summa cum laude*) from Kiel University, Kiel, Germany, in 2019.

He was an Engineer with State Grid Electric Power Research Institute, Nanjing, China, from 2007 to 2009. He was a Research Fellow and a Lecturer with the Chair of Power Electronics, Kiel University, Germany, from 2014 to 2019. He is currently an Associate Professor with the School of Electrical Engineering, Southeast University. His research interests include smart transformers, microgrid stability, modeling, and control of power converters.

Dr. Zou is an Associate Editor for the IEEE OPEN JOURNAL OF POWER ELECTRONICS and IEEE ACCESS, and an Editor for the *International Transactions on Electrical Energy Systems* and the *Mathematical Problem in Engineering.*